Experimental Comparison of EGR-VGT Control Schemes for a High Speed Diesel Engine

M.J. van Nieuwstadt I.V. Kolmanovsky P.E. Moraal

A. Stefanopoulou M. Janković

Notation

	Variables		**Subscripts**	**Constants**
p	pressure (kPa)	1	intake manifold	$c_p = 1.0144$ kJ/kg/K
T	temperature (K)	2	exhaust manifold	$c_v = 0.7274$ kJ/kg/K
m	mass (kg)	e	engine	$R = c_p - c_v$
W	mass flow (kg/s)	t	turbine	$\gamma = \frac{c_p}{c_v}$
F	burnt gas fraction	c	compressor	$\Phi_s = 1/14.4$ (stoichiometric equivalence ratio)
N	engine speed (RPM)	f	fuel	$V_d = 2.0$L engine displacement
V	volume (m^3)	a	atmospheric	
ρ	density (kg/m^3)	x	post turbine	

θ_{egr}:	EGR valve position, fraction open
θ_{vgt}:	VGT vane position, fraction open
MAF:	mass air flow
MAP:	manifold air pressure (boost)
EXMP:	exhaust manifold pressure
AFR:	air to fuel ratio
r:	EGR flow fraction

Combined subscripts, such as "e2," "12," refer to flows from the first to the second subsystem. Hence the symbol p_1, for example, refers to the intake manifold pressure in kPa and W_{c1} to the flow from compressor to intake manifold. Thermodynamic constants are those for air at 300 K.

Introduction

Diesel engine technology has made enormous strides in the areas of materials, injection equipment, and aftertreatment in the past decade. These new technologies mitigate the traditional disadvantages of diesel engines, and make them an ever more serious alternative for spark-iginited (SI) engines in the market of high performance vehicles. Diesel engines have inherently superior fuel economy compared to SI engines, however, this comes at the price of increased levels of nitric oxides, particulate matter, noise and vibration harshness (NVH), and a lower power density. Modern injection equipment allows lower emissions and NVH. The low power density is offset by the extensive use of aluminum in the engine block, head and base plate, and also by turbocharging. To achieve good boost at all speed-load conditions without sacrificing efficiency and transient performance, variable-geometry turbochargers (VGTs) are employed in high end diesel engines. These VGTs also help in controlling the trade-offs in emissions performance.

In VGTs, an actuator adjusts the angle of guide vanes placed at the entrance of the turbine to restrict the incoming exhaust gas flow. Thus different flow rates and efficiencies can be achieved at identical engine operating conditions. Exhaust gas recirculation (EGR) is used to dilute the combustion mixture, resulting

in lower peak combustion temperatures and a lower oxygen concentration and hence lower NOx emissions. Since both EGR and turbine flow are driven by the exhaust gas, there is clearly a strong coupling between the two flows. Traditional controllers ignore this coupling and use the VGT to control boost pressure and the EGR valve to control mass airflow, EGR flow, or EGR rate. A generic engine configuration with the aforementioned features is displayed in Fig. 1.

Modelling and control of diesel engines has recently generated increased interest. Diesel engine models were presented in [1, 2, 3, 4]. The particular model used here is described in [5, 6]. Different multivariable controllers were presented in [7, 8, 9, 10]. This article compares some of the control methodologies previously presented and some not yet presented to evaluate their benefits experimentally. The article does *not* include any new theory. Rather it refers to other sources for the development of the controllers evaluated here. The article *does* present an objective comparison of advanced control methodologies on a complex industrial problem with widespread application.

The control methodologies discussed are essentially *system based* i.e., the initial controller is developed on an engine *model*. An initial calibration of the controller is computed by optimization methods or by simulation of the model. Simulation is then used to assess the performance of this controller and calibration in transient operation. Model-based controller design allows for shorter development times. In particular:

- Feasibility, performance, and robustness of new control schemes can be evaluated much more readily and rapidly on the model than experimentally on the engine.
- The model can be used to aid in calibration. This reduces the often large number of calibratables to a limited number of key parameters that need to be tuned on the engine.
- Coding errors and logical inconsistencies can be caught in a modeling environment where tracing capabilities are much more refined and no risk of physical harm exists.

We use the qualifier *model based* to include controllers of conventional structure whose parameters were populated using a model. In particular, a gain scheduled PI controller with gains computed from a model would be model based. For the controllers presented here, fine-tuning of the calibration took place on the engine in a dynamometer cell.

Although a fairly obvious approach in the control community, model-based controller design is only starting to find application in the automotive industry. This can be explained in part by the limited accuracy of control-oriented power train models. Controllers developed on the basis of these models then have to be fine-tuned experimentally on the engine. Depending on the choice of control design method, this may not be a straightforward task. However, without this fine-tuning, the controller may not perform acceptably at some operating points. Thus, this article focuses on the experimental validation and ease of calibration of various model-based control designs.

Although the control designs are based on different ideas, the objectives of these designs were to improve robustness and performance of closed-loop operation and to decrease calibration complexity. The controllers are assessed on their emissions and fuel economy on the extra urban drive cycle (EUDC) of the eurocycle. The experimental conditions under which the controllers were evaluated differ from a vehicle chassis role test used in homologation in many respects: the dynamometer does not respond the way a vehicle does, shift transients are different, there may be problems with shaft vibrations, and engine knowledge is incomplete. In practice, controller design happens in parallel with vehicle and engine specification, and a decision on controller architecture has to be made more often than not based on incomplete hardware knowledge. Hence for a system based control design approach to be useful in the automotive industry, it is imperative that controllers can be assessed early in a program when the whole system has not necessarily been defined. Robustness is then a crucial property that allows the controller to work correctly when the hardware further evolves. The controllers are also evaluated on their ease of calibration and implementation and computational load in production hardware, since these are major cost factors in controller implementation.

The development of this article is as follows. First we describe the rapid prototyping enviroment used for our experiments. Some of the controllers estimate the controlled variables, and this estimator is described next. The generation of the set points for the controllers is performed on the model and presented next. This is followed by some detail on the various control methodologies that are the subject of our comparison. Cumulative emission numbers on the EUDC are given first, then transient plots are presented. Finally we summarize our findings and present conclusions.

Hardware Setup

Fig. 1 shows the engine that is the subject of this investigation, a 115-HP direct-injected diesel engine with four valves per cylinder, a VGT and external EGR. A dSPACE rapid prototyping system is at the heart of our setup; it was used to implement the controllers, monitor their performance, and interface to various other control modules. The various components of this setup are shown in Fig. 2. In the production environment, the engine is controlled by an engine control unit (ECU) in conjunction with an injection control unit (ICU), communicating over a controller area network (CAN) link [11]. The ECU sends fueling commands (timing and quantity) to the ICU, which executes these commands. The ICU contains the hardware drivers for the injectors. In addition to fueling information, various diagnostics messages are sent to guarantee safe operation of the system. The ECU normally also controls the other actuators of the engine, in particular, the EGR and VGT, monitors the health of the engine, and processes sensor input.

In our setup, we cut the CAN link between the ECU and ICU and put a dSPACE CAN board on each end. The dSPACE system passes all CAN messages verbatim, with the possible exception of fuel quantity and timing. This allows one to apply controller fuel steps from dSPACE as external disturbances to the air management system and to run transient cycles. The air management control of the ECU is bypassed and is directly controlled by the dSPACE rapid prototyping system. This system has as measured inputs engine speed, intake manifold pressure (boost), mass airflow (MAF), exhaust manifold pressure, air charge temperature (ACT), VGT vane position and EGR valve position, and commanded fuel quantity. Its control outputs are EGR valve duty cycle and VGT vane position duty cycle. The PWM duty cycles are input to a current amplifier and sent to the current-to-vacuum transducers (CVTs) that control the EGR and VGT actuators.

The dSPACE system also controls the dynamometer speed and load through analog output voltages. This allows control of transient cycles: the fuel command is used as feedforward, and torque and engine speed are controlled through a simple PID loop. As indicated above, the controllers are first tested on a mean value model [5] in the MATLAB/Simulink environment. The same code is then run on the dSPACE Autobox to control the engine. Use of the dSPACE/MATLAB/Simulink environment considerably shortened the test time and was essential to providing the ability to interface with all the different components.

Estimation of MAF and EGR Flow

Some of the controllers discussed in this article use an estimation scheme to generate several signals that were not measured. This estimation scheme is briefly described here.

The estimator is used for controllers that assume availability of an intake manifold pressure (MAP or p_1) and an exhaust manifold pressure (EXMP or p_2) sensor. This choice of sensor is less costly than the standard choice of sensor for MAP and compressor mass airflow (MAF). From the ideal gas law, we have, under the isothermic assumption,

$$\dot{p}_1 = \frac{RT_1}{V_1}\big(W_{21} + W_{c1} - W_{1e}\big), \tag{1}$$

where W_{21} is the flow through the EGR valve, W_{c1} is the flow through the compressor, W_{1e} is the intake flow to the engine, T_1 is the intake manifold temperature, and V_1 is the intake manifold volume. If the exhaust manifold pressure and temperature are known or can be estimated from open loop maps, we can calculate the EGR flow from the orifice flow equation

$$\begin{aligned} W_{21} &= C_d(\theta_{\text{egr}})\frac{p_2}{\sqrt{RT_2}}\Psi\left(\frac{p_1}{p_2}\right), \\ \Psi(x) &= \sqrt{\frac{2\gamma}{\gamma-1}\left((x)^{\frac{2}{\gamma}} - (x)^{\frac{\gamma+1}{\gamma}}\right)} \text{ for } x > \left(\tfrac{2}{\gamma+1}\right)^{\frac{\gamma}{\gamma-1}}, \text{and} \\ \Psi(x) &= \gamma^{\frac{1}{2}}\left(\frac{2}{\gamma+1}\right)^{\frac{\gamma+1}{2(\gamma-1)}} \text{ for } x \le \left(\tfrac{2}{\gamma+1}\right)^{\frac{\gamma}{\gamma-1}}, \end{aligned} \tag{2}$$

and $C_d(\theta_{\text{egr}})$ is a function of EGR valve position, θ_{egr}, developed from steady-state engine mapping data. The engine intake flow is calculated from the volumetric efficiency of the engine η_V, engine speed N, and

engine displacement volume V_d as

$$W_{1e} = \frac{\eta_V \rho_1 V_d N}{120}, \qquad \rho_1 = \frac{p_1}{RT_1}. \tag{3}$$

From (1) we obtain

$$W_{c1} = \frac{V_1}{RT_1}\dot{p}_1 - W_{21} + W_{1e}. \tag{4}$$

We can approximate $\dot{p}_1$ with a numerical differentiation filter

$$\bar{\dot{p}_1} = \frac{s}{\tau s + 1}\, p_1, \tag{5}$$

with suitable time constant τ. This time constant has to be chosen as small as possible without excessively amplifying noise. Then, by low-pass filtering the flows:

$$\bar{W}_{21} = \frac{1}{\tau s + 1} W_{21}, \qquad \bar{W}_{1e} = \frac{1}{\tau s + 1} W_{1e} \tag{6}$$

we obtain

$$\hat{W}_{c1} = \frac{V_1}{RT_1}\bar{\dot{p}_1} - \bar{W}_{21} + \bar{W}_{1e}. \tag{7}$$

This gives an estimate for MAF.

Figure 3 show MAF and its estimate over the extra urban part of the European drive cycle. It shows that the estimator underestimates MAF in transients, which has the beneficial side effect of providing extra air in transients, leading to a faster torque response. The figure also shows that there are steady state errors, which could be handled by offsetting the MAF set points.

Set points

Feedback controllers for diesel engine management are most typically implemented as regulators. The performance variables, such as emissions, fuel consumption and torque response, can usually not be measured in a production implementation, due to prohibitive cost. Hence a measureable variable with some correlation to the performance variable is used instead. The set point for these variables is determined from a lookup table or polynomial approximation over speed and fuel quantity, the latter being a close indication of load. With some abuse of terms, we will refer to fuel quantity as "load" in this development. The task of the feedback controller is then to control the actuators such that the measured variables are driven to their respective set points. We emphasize here that the feedback controller can only be expected to control transient performance and to provide robustness against external disturbances and system uncertainty. If the set points do not meet the emissions and fuel consumption targets in open loop, the feedback controller cannot be expected to improve the closed loop behavior of the engine. The set points are therefore of crucial importance. This is especially true when the engine performance is evaluated over the European drive cycle, which contains long stretches of steady state operation. The present section will detail the calculation of the set points used for the controllers in this article.

Let Z_i denote our performance variables, that is emissions and fuel consumption for a *fixed* speed load point, and let Y_i denote the measured variables. In this article we also fix start of injection, so that for a fixed speed load point, our remaining control variables are EGR valve command θ_{egr} and VGT command θ_{vgt}. We combine the performance variables in a single cost criterion to be minimized:

$$J(\theta_{\text{egr}}, \theta_{\text{vgt}}) = \sum_i \lambda_i Z_i(\theta_{\text{egr}}, \theta_{\text{vgt}}),$$

where λ_i indicates the weight we assign to performance variable Z_i. By changing the factors λ_i we achieve a different trade-off between different emission species and fuel economy.

The calculation of set points is now to find EGR and VGT commands that minimize J, and then the values of the measured variables Y_i that correspond to these commands. This minimization could in principle be performed by standard optimization software. Since the model does not give the performance variables as closed form functions of the actuator settings, each iteration would involve a simulation of the system, keeping speed and load constant, and applying an open loop actuator effort until the system has reached steady state. Since this is a computationally expensive procedure, one often resorts to a simpler alternative, which is detailed in the sequel. Fortunately, the cost functions for our problem are mostly well behaved, and one can get reasonable results by collecting some data n-tuples $(\theta_{\text{egr}}, \theta_{\text{vgt}}, Y_i, Z_i)$ for fixed speed and load, and regressing Z_i and Y_i locally as a polynomial in θ_{egr} and θ_{vgt}. These n-tuples can be gathered from an engine dynamometer or a high fidelity simulation model. As an example, if we aim to minimize brake-specific fuel consumption (bsfc) as a quadratic function of EGR and VGT, we compute a least-squares fit of the coefficients c_i in the expression

$$\text{bsfc} = c_0 + c_{1e}\theta_{\text{egr}} + c_{1v}\theta_{\text{vgt}} + c_{2e}\theta_{\text{egr}}^2 + c_{2v}\theta_{\text{vgt}}^2 + c_{2ev}\theta_{\text{egr}}\theta_{\text{vgt}},$$

and can easily find the optimal θ_{egr}^* and θ_{vgt}^* that minimize BSFC. Similarly, one can regress the measured variables Y_i as quadratic functions of the θ_{egr} and θ_{vgt}, and substitute the optimal actuator settings θ_{egr}^* and θ_{vgt}^* to arrive at the set point for Y_i, denoted Y_i^*. This procedure is repeated for several speed load points, as many as necessary to obtain a set point matrix of the desired resolution in speed and load.

It may happpen that an l_∞ constraint needs to be applied to either performance variables Z_i or actuator settings. This can be handled by only using those n-tuples $(\theta_{\text{egr}}, \theta_{\text{vgt}}, Y_i, Z_i)$ in the regression that satisfy the constraint. This is not a fail-safe way to guarantee that the resulting optimal $(\theta_{\text{egr}}*, \theta_{\text{vgt}}*, Y_i^*, Z_i^*)$ satisfy the constraint, but it usually is a good start.

Applying this simplified procedure to minimze BSFC as a function of θ_{egr} and θ_{vgt} while restricting smoke to be invisible (less than 2 BSU), we arrived at set points for MAP and MAF for the PI controllers on MAP and measured or estimated MAF. This procedure was also applied to arrive at set points for the PI controller MAP and EGR fraction.

The controller in described under "Rank One Controller" was designed specifically for set points that minimize feedgas NOx emissions by maximizing the burnt gas fraction F_1 in the intake manifold. This addresses the high NOx emissions common to diesel engines. To avoid excessive smoke, the air fuel ratio was constrained to be sufficiently lean. Although, the minimum AFR level is a function of the fueling rate and engine speed, we chose for simplicity the fixed value of $textAFR_{min} = 25$. A second constraint is imposed on maximum intake manifold pressure to protect the engine from damages due to over-boost. The assumed maximum intake manifold pressure is $p_{1max} = 220$ kPa.

The CLF controller decribed later used set points based on the EGR fraction set points from a production engine of similar displacement to the one under investigation in this article, and AFR set points that were proven feasible in simulation. The EGR and AFR set points where mapped to set points for the measured variables MAF and EXMP using the engine model.

Since no engine mapping data for speeds lower than 1500 RPM was available, we generated set points for these speeds by extrapolation. Thus it cannot be assured that these set points are feasible, let alone optimal. It is of course a sign of increased robustness if a controller can still control the controlled variable to its set point outside of the mapped speed load range.

Controllers

The following control strategies are described in this section and evaluated in the next section:

- Decentralized proportional-integral (PI) control of MAP and measured MAF, using MAP and MAF sensors to generate duty cycle commands for EGR and VGT.
- Decentralized PI control of MAP and estimated MAF, using MAP and exhaust manifold pressure sensors to generate duty cycle commands for EGR and VGT.
- Rank one PI control (R1) of MAP and MAF, using MAP and MAF sensors to generate *position* commands for EGR and VGT.

- Multivariable linear proportional control of MAF and EXMP generating *position* commands for EGR and VGT. This controller is derived from a control Lyapunov function, hence we will refer to it as a CLF controller.
- Decentralized PI control of MAP and EGR flow fraction, using MAP and EXMP sensors to generate duty cycle commands for EGR and VGT.

Note: The controllers that generate *position* rather than *duty cycle* commands require additional EGR and VGT position sensors and corresponding inner-loop controllers to generate the final duty cycle command signal to the actuators. Due to nonlinear dynamics and hysteresis, it is difficult to map position commands to duty cycle commands in open loop fashion.

Table 1 summarizes the distinguishing features of the controllers. The qualification "coupled" refers to the property that an error in one controlled variable will produce control effort in both actuators. All controllers are indirectly coupled through the plant.

The controllers that replace a MAF sensor with an EXMP sensor offer a potential cost benefit. However, the EXMP sensor may have durability problems in production due to soot deposits prevalent in diesel exhaust manifolds.

Intake manifold pressure and mass airflow

A conventional controller for this engine would use feedforward combined with PI control on MAP and MAF, as depicted in Figure 4.

The VGT vanes control MAP and the EGR valve controls MAF. The values for each of the four PI gains are stored in a table, over engine speed and fueling rate. The controller parameters are tuned by hand. Although it should be mentioned that, in practice, blocks of cells are tuned, effectively reducing the resolution, this is still a formidable calibration task. We used tables of size 6×7 and generated PI gains by scaling the inverted plant dc gain at different operating points. If the dc gain of the plant from (VGT, EGR) duty cycles to (MAP, MAF) is $K_{dc}(N, W_f)$, and $K_g = K_{dc}^{-1}$, we set the proportional gain as

$$K_p(N, W_f) = \begin{pmatrix} k_{p11} K_{g11}(N, W_f) & 0 \\ 0 & k_{p22} K_{g22}(N, W_f) \end{pmatrix}, \tag{8}$$

and we set the integral gain as

$$K_i(N, W_f) = \begin{pmatrix} k_{i11} K_{g11}(N, W_f) & 0 \\ 0 & k_{i22} K_{g22}(N, W_f) \end{pmatrix}. \tag{9}$$

Here K_{gij} represents the (i, j)-th element of the matrix K_g that we generated from steady-state engine mapping data, or from the model. The gains k_{p11}, k_{p22}, k_{i11}, and k_{i22} are the same for all operating points and are tuned on the engine. The variability with operating point comes from the inverse of the dc gain. Only four gains had to be tuned on the engine, presenting a considerable savings compared to conventional practice.

The code implementing the strategy does not contain any part of the engine model, thereby reducing the chronometric load and implementation effort. Since only four gains had to be tuned, the calibration task is modest.

In experiments, we used the following antiwindup strategy. The contribution of the integral term was limited to a certain threshold value. If this value threatened to be exceeded, integration would stop until the integral term came within bounds. The threshold was set to 20 % duty cycle for both EGR and VGT. That means that the feedforward and proportional control should drive the actuator to within a band of 20 % of the right value.

Intake manifold pressure and estimated mass airflow

The controller architecture is exactly the same as described above, except that MAF is not measured but is estimated from MAP and an exhaust manifold pressure measurement as detailed under "Estimated Signals". The estimate of MAF is fed to the controller in place of measured MAF. The architecture is as in Figure 4, with measured MAF replaced by estimated MAF.

The MAF estimation requires the implementation of the scheme outlined in Section , thus increasing the chronometric load. The calibration task is the same as for the PI controller on MAP and MAF.

Rank one controller

The control design objective is to coordinate the actuators with the control input $u = \left[\begin{array}{cc} \theta_{\rm egr}, & \theta_{\rm vgt} \end{array} \right]^{\rm T}$ to (i) speed up the engine open loop dynamics in order to reduce transient AFR excursions, and (ii) to regulate AFR and F_1 close to a new setpoint according to the maximum F_1 strategy. The performance variables are not measured directly, and the control scheme relies on the measurements of MAF and MAP, i.e., $y = \left[\begin{array}{cc} MAF, & MAP \end{array} \right]^{\rm T}$. The characteristics of the engine behavior at these maximum F_1 operating points dictate a multivariable controller architecture that is rank one. We summarize next the characteristic feature of the open loop plant that dictate this special controller architecture, the implications of this feature in the feedback control design, the design of a feedback controller that directly addresses the open loop plant characteristic at the maximum F_1 operating points. Detailed discussion of the nominal and robust properties of the closed loop system, as well as simulation and experimental results can be found in [8] and [10].

The rank one controller configuration is shown in Fig. 5. The error, $\tilde{e}$, which is fed to the PI controller is formed as a linear combination of MAF and MAP errors, with weights h_1 and h_2. The signal generated by the controller, $\tilde{u}$, is distributed to EGR and VGT position commands through weights g_1 and g_2. The commands for EGR and VGT positions are then fed to the inner-loop PI controllers that generate duty cycle inputs for the actuators. The scheme is a particular way of coordinating EGR and VGT actuators.

The rationale for the proposed arrangement is best understood by considering the linearization of the plant model at a given operating point where the control signal is $u = [\delta EGR, \quad \delta VGT]^{\rm T}$, the measured output is $y = [\delta MAF, \quad \delta MAP]^{\rm T}$ and the performance output is $z = [\delta F_1, \quad \delta AFR]^{\rm T}$. The output z is chosen as a performance output because it has strong influence on emissions such as smoke and NOx. The objective is to drive z to a value which is, indirectly, specified by the set-point for the measured output, y_d.

Let P_y denote the dc-gain of the plant from the input u to the output y and let P_z denote the dc-gain from the input u to the output z. The development is motivated by the fact that the matrix P_z is "almost" singular, and P_y is "very" regular. This property holds at the operating points corresponding to the maximum F_1 strategy (see Section). The controller was designed to operate primarily with this strategy. The intuitive reason for this property is clear: when the burnt gas fraction increases, the fresh air charge is displaced from the intake manifold and the in-cylinder air-to-fuel ratio decreases.

Let us now consider the singular value decomposition (SVD) of $P_z(0)$:

$$P_z(0) = \sigma_1 w_1 v_1^T + \sigma_2 w_2 v_2^T \tag{10}$$

where σ_1 and σ_2 are the largest and smallest singular values of $P_z(0)$, and (w_1, w_2) and (v_1, v_2) are the corresponding sets of left and right singular vectors, respectively. For our problem, $P_z(0)$ is "almost" rank deficient, in the sense that it has both a large condition number ($\kappa \approx 64$) and a small singular value ($\sigma_{min} \approx 0.04$). Furthermore, scaling cannot alter the underlying redundancy as shown in [10]. It follows that relatively small commands may result in large control signals. On the other hand, commands that satisfy $\delta z^* \in \mathbf{R}(w_1)$ may be tracked without using large control signals; we say that such commands lie in the "effective range" of the plant and we refer to them as *"feasible"*. A controller with an integrator for each input-output pair (or, simply, high-gain) will thus achieve perfect steady state tracking of all commands at the expense of large control signals, which are undesirable because they may result in frequent actuator saturation.

Notably, the operating point defined by the triple $\left[\begin{array}{ccc} u_B & z_B & y_B \end{array} \right]$ shows that the actuator redundancy dissappears as the operating point moves inside the *performance range*. Thus, one can design a high-gain controller augmenting the plant with 2 integrators if we do not require operation at the maximum F_1 strategy for a given AFR constraint. This explains why the all the other controller structures, decentralized PI and CLF controllers, did not face any serious difficulties in regulating to their corresponding set points. Indeed, both the minimum fuel economy and the EGR fraction set points correspond to internal points in the *performance range* with full rank open loop plants.

Note that the problem of actuator redundancy is caused by the necessity to operate at optimized operating points. In addition, the fact that we have optimized the performance variables implies that the desired operating points tend to lie on the boundary of the *performance range*. In light of the difficulties that these operating points impose to the feedback controller design, a possible solution is to generate a different set-point strategy that results in engine operation away from "optimal" but "difficult" set points. However, this solution would degrade feedgas NOx emission performance of the engine and may be undesirable due to the very stringent NOx emission regulations currently being put in place. In light of the redundancy, a simple controller architecture could utilize only one actuator and track only one set-point variable. The decision of

which pair of signals should be utilized by the controller can be determined based on actuator reliability or sensor cost. Another approach is to design a rank one controller that utilizes both actuators and ensures maximum control authority.

The rank one controller configuration is shown in Figure 5. The fictitious error, $\tilde{e}$, which is fed to the PI (or a high-gain) controller is formed as a linear combination of th measured MAF and MAP errors, with weights h_1 and h_2, which are designed to reduce the impact of strategy errors by not attempting to track infeasible set points. The signal generated by the PI controller, $\tilde{u}$, is distributed to EGR and VGT position commands through weights g_1 and g_2 that are designed to coordinate the actuators to achieve maximum authority. The commands for EGR and VGT positions are then fed to the inner-loop PI controllers that generate duty cycle inputs for the actuators. The PI controller gains K_p and K_i are fixed throughout the operating range and need only be tuned at a single operating point. We briefly describe the control design and properties here.

Let the rank one controller be $C(s) = GK_C(s)H$ where $H = [h_1 \;\; h_2]$ and $G = [g_1 \;\; g_2]^T$ are constant matrices in $\mathbf{R}^{2\times 1}$ and where $K_C(s) = K_p + \frac{K_i}{s}$ is a PI controller. We choose H so that the controller attempts to track only those y-commands corresponding to z-commands that lie in the effective range of $P_z(0)$:

$$H = w_1^T P_z(0) P_y^{-1}(0) / \| w_1^T P_z(0) P_y^{-1}(0) \|. \tag{11}$$

The transfer function mapping y-commands to the control signal is given by $C(s)\left(I + P_y(s)C(s)\right)^{-1}$ and has dc gain of magnitude $\|GH\|/|HP_y(0)G| = \|Gw_1^T P_z(0)P_y^{-1}(0)\|/|w_1^T P_z(0)G|$. Because $w_1^T P_z(0)G = \sigma_1 v_1^T G$, it is easy to verify that choosing $G = v_1$ minimizes the size of the steady-state control signal. Indeed, a small step change in reference command can be decomposed into the part that belongs to the effective range of $P_z(0)$ (feasible component) and its orthogonal complement with appropriate scalars α_1 and α_2:

$$\delta y^* = \underbrace{\alpha_1 P_y(0)P_z(0)^{-1}w_1}_{\text{feasible component}} + \alpha_2 P_y(0)P_z(0)^{-1}w_2. \tag{12}$$

This reference command will generate the steady-state control signal

$$\begin{aligned} \delta u_{ss} &= GH\delta y^* / (HP_y(0)G) \\ &= v_1 w_1^T P_z(0) P_y(0)^{-1} \delta y^* / (HP_y(0)G) \\ &= \alpha_1 v_1 / \sigma_1. \end{aligned} \tag{13}$$

Moreover, the combination of H and G ensures that the *smallest* control signal will be used to achieve steady state tracking of the component of δy that corresponds to the effective range of the performance variables. Indeed, consider the control signal from (13), then the measured output is

$$\delta y_{ss} = P_y(0)\delta u_{ss} = \alpha_1 P_y(0) v_1/\sigma_1 = \alpha_1 P_y(0) P_z(0)^{-1} w_1,$$

which is the feasible component of the reference input.

Preliminary evaluation of the controller on fuel steps at 1500 rpm has demonstrated a time constant of MAF response of about 0.2 sec. Fast transient performance is important for turbo-lag reduction, which is a large concern in diesel engines. Moreover, as the load increases, the controller tends to open the VGT in coordination with closing the EGR. This tends to keep engine backpressure small, thereby providing good fuel economy.

As the experimental data in we will show later indicate, due to model uncertainty the air-to-fuel ratio went as low as 20 in steady state. This indicates the need for a more conservative $\text{AFR}_{min} = 30$ value in the future development of maximum F1 strategy set points.

The code implementing the strategy does not contain any part of the engine model, thereby reducing the chronometric load and implementation effort. The matrices G and H are based on the SVD of the dc gain of the engine model at different operating points that span the maximum F1 strategy. Since only the two gains K_p and K_i had to be tuned, the calibration task is modest.

CLF controller

This controller was developed using a design method proposed in [12] that applies to nonlinear multivariable systems for which a control Lyapunov function can be constructed. The motivation for considering this method is that it provides a robustness guarantee equivalent to linear SISO gain and phase margins.

Our control objective is to regulate the in-cylinder air-to-fuel ratio, defined by

$$AFR = (1 - F_1)W_{1e}/W_f,$$

where F_1 is the burnt gas fraction in the intake manifold, and the flow fraction

$$r = W_{21}/(W_{c1} + W_{21}), \tag{14}$$

to their desired set point values appropriate for the current operating conditions (engine speed and driver fuel request W_f^d). Due to limited time available to develop set points for this controller, the desired set points,

$$AFR^d(N, W_f^d) \quad \text{and} \quad r^d(N, W_f^d),$$

have been obtained by taking an EGR schedule for a different, 1.9-liter turbocharged diesel engine and, somewhat arbitrarily, scheduling the air-to-fuel ratio to get feasible operating points in simulations on a 2.0L diesel engine model. Because no experimental data were available to validate the model in the low-speed region, the set points have only been obtained and stored for engine speed values between 1500 and 3000 RPM and for fueling rates that exceed 1 kg/hr. Outside this region the set points are generated by extrapolation and are, in general, infeasible.

Because neither AFR nor r can be directly measured, we transformed these set points into the desired set points for MAF (W_{c1}^d), MAP (p_1^d), and EXMP (p_2^d):

$$\begin{aligned} W_{c1}^d &= W_f^d\ [AFR^d(1 - r^d) + 14.6\ r^d], \\ p_1^d &= \frac{W_{c1}^d}{k_e(1 - r^d)}, \\ p_2^d &= p_a \left(1 - \frac{W_{c1}^d}{W_{c1}^d + W_f^d}\ \frac{T_a}{T_2 \eta^*}((\frac{p_1^d}{p_a})^\mu - 1)\right)^{-\frac{1}{\mu}}, \end{aligned} \tag{15}$$

where $\mu := \frac{\gamma - 1}{\gamma} = 0.286$, k_e is the engine pumping coefficient (defined as W_{1e}/p_1, proportional to volumetric efficiency), assumed here to be a function of engine speed only, $\eta^* := \eta_m \eta_{c,is} \eta_{t,is}$ is the total efficiency of the turbocharger, p_a is the ambient pressure, and T_a is the ambient temperature. For simulations and dynamometer testing, the set points (15) have been computed using $k_e = \alpha_1 N$, $\eta^* = \alpha_2 + \alpha_3 W_f^d$, and $T_2 = \alpha_4 + \frac{\alpha_5}{AFR^d}$, with α_i, $i = 1, \ldots, 5$, being positive constants chosen to match approximately the behavior of the engine model.

A CLF, required for this design method, has been constructed using input-output linearization of a simplified third-order diesel engine model. The EGR mass flow rate W_{21} and the turbine mass flow rate W_{2t} are considered the inputs to the system and denoted by v_1 and v_2, respectively. The two outputs for feedback linearization, $y_1 := W_{c1} - W_{c1}^d$ and $y_2 := p_2 - p_2^d$ (not necessarily the measured signals), have been selected so that the system is "minimum-phase." This property is required for input-output linearization to produce a stabilizing control law and may also have a positive effect on the performance and robustness of the closed-loop system.

The controller design proceeds through steps of input-output linearization, construction of a CLF, and domination redesign, which provides the final control law. Details can be found in [13, 7]. The resulting control law takes the form

$$\begin{aligned} v_1 &= \frac{r^d}{1 - r^d} W_{c1}^d - \gamma_1 \left(-c_1 a(W_{c1} - W_{c1}^d) - c_2 k_2 (p_2 - p_2^d) + c_3 k_2 \mu p_1^{\mu - 1}(p_1^\mu - (p_1^d)^\mu)\right), \\ v_2 &= (W_{c1}^d + W_f^d) - \gamma_2 \left(c_1 b(W_{c1} - W_{c1}^d) - c_2 k_2 (p_2 - p_2^d)\right). \end{aligned} \tag{16}$$

The coefficients a and b were derived as nonlinear functions of the states, but to simplify the controller, we have fixed their values to be constant. The gain k_2, which is defined as $\frac{RT_2}{V_2}$, is also kept constant in the controller. The parameters $\gamma_1, \gamma_2, c_1, c_2, c_3$ are the adjustable gains of the controller. These gains have been selected based on extensive simulations. As a result, the gain c_3 has been set to zero (that is, the MAP feedback has been turned off). This has left the control law (16) a linear proportional multivariable (cross-coupled) feedback in compressor air flow and the exhaust manifold pressure regulation errors:

$$\begin{aligned} v_1 &= v_1^d + \kappa_{11}\ (W_{c1} - W_{c1}^d) + \kappa_{12}\ (p_2 - p_2^d), \\ v_2 &= v_2^d - \kappa_{21}\ \delta(W_{c1} - W_{c1}^d) + \kappa_{22}\ (p_2 - p_2^d) \end{aligned} \tag{17}$$

where $v_1^d = \frac{r^d}{1-r^d} W_{c1}^d$ and $v_2^d = W_{c1}^d + W_f^d$ are the set points for the EGR valve and turbine flows and $\kappa_{ij} > 0$ are the proportional gains. Once the "inputs" $v_1 = W_{21}$ and $v_2 = W_{2t}$ are computed, appropriate orifice flow relationships of the form (2) are inverted to obtain the desired EGR valve position θ_{egr} and VGT vane position θ_{vgt}. Note that this inversion becomes ill-conditioned for low pressure drops. Indeed, a considerable amount of dynamometer time was spend to regularize these inversions. The position values are then commanded to the inner loop controllers for the two actuators. We believe that this extraction of the nonlinearities contained in the maps $\theta_{egr} \to W_{21}$ and $\theta_{vgt} \to W_{2t}$, allowed the system to be controlled by fixed-gain linear feedback (17). The configuration of the CLF controller is shown in Figure 6.

added this. MvN

The CLF controller design specifically targets fast air flow response which is important for turbo-lag reduction. The faster the increase in the compressor air-flow, the smaller the delay between driver's demand and fuel (torque) delivery for larger tip-ins. Preliminary experimental evaluation of the controller at engine speeds above 1500 rpm has shown a MAF response time constant of 0.16 sec or less, independent of engine speed. MAF and EXMP signals correspond to the minimum-phase outputs, so the achievable response speed is not limited by the presence of unstable zeros. The gains that can be used are limited by the unmodeled actuator dynamics and by Butterworth filters used to filter out measurement noise (20 rad/s bandwidth). *The latter limitation can be reduced, and possibly completely removed, if the sampling is crank angle based. In the current hardware setup sampling is time-based, so the Butterworth filters had to be used.*

took this (crank sync sampling) out, doesn't make sense for diesel mvannie1

Integral action could have been added to one or both of the output channels. This has not been done for two reasons: (*a*) addition of integrators would have likely slowed down the air flow response possibly increasing the turbo-lag; (*b*) a degradation in performance and even stability loss may result for a MIMO architecture due to VGT-to-MAF dc gain reversal if the set points are infeasible. The steady-state error is reduced by selecting gains of the proportional feedback that are high enough.

The code implementing the strategy contains EGR and turbine orifice flow models, thereby increasing the chronometric load. On the other hand, the controller does not require gain-scheduling, thus reducing memory usage compared to other control designs. On a fixed-point processor, the nonlinear functions occurring in the orifice flow inversion would have to be approximated by table look-up reducing the chronometric load, but increasing memory usage. Since only four gains would have to be tuned for experimental calibration, the calibration task is modest. Due to the lack of integral control, the steady-state error depends on the magnitude of the proportional gain.

Intake manifold pressure and EGR flow fraction controller

Like the PI controller on MAP and *estimated* MAF this controller was developed to address the situation where an EXMP sensor and a MAP sensor are available but a MAF sensor is absent. In this situation, available sensor measurements can be used to estimate EGR flow and MAF as detailed under "Estimated Signals." If MAP and MAF sensors are available but not an EXMP sensor, the controller can still be used. The estimate of EGR flow required for this mode of operation can be generated using an algorithm similar to the one we use to estimate MAF from MAP and EXMP measurements. If EXMP and MAP are measured, errors in estimating MAF may exceed those in estimating EGR flow. The controller evaluated here uses estimated (as opposed to measured) MAF to calculate the EGR rate set points.

The controller architecture is the same as depicted in Fig. 4), except that the controlled variables are now MAP (which is measured) and EGR flow *fraction*, r, defined as the ratio of EGR flow (W_{21}) to the sum of EGR flow and MAF (W_{c1}), Eq. (14). Of course, the EGR flow fraction is not directly measured by sensors but is estimated. There are two decentralized loops: one from the VGT actuator duty cycle to MAP and one from the EGR valve actuator duty cycle to EGR flow fraction. Just as for the MAP/MAF controller, only four gains need be tuned on the engine. These gains are then scaled by coefficients depending on engine speed and fueling rate that are generated from engine steady-state mapping data. These details and those of the antiwindup compensation are exactly the same as for the MAP/measured MAF controller.

The choice of the controlled outputs deserves some discussion. Initially, we considered selecting EGR flow, W_{21}, as the second controlled output. The motivation for this choice was twofold. First, small errors in MAF sensor calibration or MAF estimation may translate into large errors in EGR flow and thus poor emissions performance. Secondly, during phases where the driver demands a large acceleration, it is critical to reduce EGR flow as quickly as possible so that the engine is provided with as much fresh air charge as possible. The actuators have a more direct effect on EGR flow than on MAF and can reduce it quickly when commanded to do so. Unfortunately, the selection of EGR flow as a controlled output has a very important drawback. We found it very advantageous if the steady-state map from actuator to measured

variable is monotonic over the engine operating range. That is, regardless of the operating point, increasing the actuator effort will always increase (or decrease) the value of the controlled variable. If this is not the case, the controller gains have to change sign depending on the operating point. Since the point where a sign change occurs is never known precisely, this means that in certain operating ranges, the controller gains will be of the wrong sign, with obvious disastrous results. The gain from VGT to MAF, for example, changes gain from positive at low engine speed to negative at high engine speed. Similarly, the gain from EGR valve duty cycle to EGR flow changes sign, albeit in small operating ranges with the EGR valve almost entirely open. This can be explained from the decrease in exhaust manifold pressure that occurs with opening the EGR valve. Consequently, we decided to use EGR flow fraction, r, as the second controlled output. It was confirmed that the dc gain from EGR valve position or EGR valve duty cycle to EGR flow fraction is always positive. The dc gain from VGT actuator position or VGT actuator duty cycle to MAP does not change sign either.

The code implementing the strategy does contain the orifice flow equation (2) to compute the estimated MAF, increasing the chronometric load and implementation effort. Since only four gains had to be tuned, the calibration task is modest.

Dynamometer Data

Drive cycle

The controllers were tested on the extra urban driving cycle of the eurocycle (i.e., the last 400 sec). As mentioned earlier, we did not have mapping data for low engine speeds, hence the higher engine speeds of the EUDC better reflected the design methodologies.

To simulate the drive cycle we need to control engine speed and load torque. The torque was regulated through a PI controller using low pass filtered shaft torque as an input, and controlling the fuel rack position as an output. The commanded engine speed was sent as a voltage to the dyno controller, which uses an internal feedback loop to control speed. The dyno controls engine speed with the electric brake. Since this internal feedback is of high bandwidth, tracking engine speed is no problem.

We used a MATLAB model of a Ford Mondeo to compute the engine speed and load from the vehicle speed and gear strategy. Fig. 7 shows the vehicle speed, engine speed, engine torque, and requested fuel for the EUDC.

Particulate emissions

Since a direct particulate measurement was not available, we use a correlation that expresses particulate matter as a function of smoke and hydrocarbons proposed by [14]. This method relies on an expression for carbon concentration proposed by [15]:

$$[C]_{kg/m^3} = 581.4\,10^{-6}(\log(\frac{10}{10-Bn}))^{1.413} \tag{18}$$

and a linear correlation proposed by [16]:

$$[PM]_{kg/s} = 1.024\,[C]_{kg/s} + 0.505\,[HC]_{kg/s}, \tag{19}$$

where Bn is the smoke number in Bosch smoke units and [HC] is the mass flow of hydrocarbons in the exhaust gas in kg/s. To convert the carbon concentration from kg/m^3 to kg/s, we assume steady-state relations hold, in which case $W_{2x} = W_{c1}$. With the density of the exhaust gas in kg/m^3, expressed in post turbine pressure p_x in kPa and post turbine temperature T_x in Kelvin, as follows:

$$\rho_x = \frac{p_x}{RT_x}, \tag{20}$$

we get

$$[C]_{kg/s} = \frac{[C]_{kg/m^3} \cdot W_{c1,kg/s}}{\rho_x}. \tag{21}$$

Substituting (21) into (19) gives the desired quantity. This expression has limited quantitative accuracy but is a useful qualitative measure.

Controller statistics

For each controller, we calculate the total NOx, HC, CO, and PM emissions and the total time in seconds that smoke was visible (> 2 BSU). Care has to be exercised in interpreting these results. First, one should keep in mind that we are dealing with feedgas emissions and not tailpipe emissions. Exhaust aftertreament will change the numbers for tailpipe emissions considerably. Second, as we will see, the set points have a large influence on the resulting emission and fuel economy numbers, and not all controllers were evaluated on the same set points.

The results are normalized with respect to open-loop operation and tabulated in Table 2. The rank one controller using maximum F_1 set points produced excessive smoke, since these set points try to maximize EGR content in the intake manifold, and a small positive error in F_1 will lead to visible smoke. The set points for the maximum F_1 strategy were developed on the model, and discrepancies between the model and the engine, even at mapped engine speeds, can be responsible for this behavior. The rank one controller also produced considerably more CO than the other controllers. This points at incomplete combustion which correlates with the high smoke numbers. The engine running in open-loop produced excessive NOx. The CLF controller on AFR and EGR fraction also produced visible smoke for 1.8 sec, and the PI controller on MAP and measured MAF produced visible smoke for 0.05 sec.

It is extremely interesting to plot NOx against particulate emissions as is done in Fig. 8, where the particulate matter emissions were calculated as detailed above. This illustrates the well-known NOx-particulate tradeoff which is a fundamental limitation of the diesel combustion system. Diesel combustion is an extremely complex interaction between mixing dynamics and chemistry, but a intuitive, albeit very approximate, explanation can be given for this tradeoff. Increased air fuel ratio improves combustion speed and quality to a ceratin extent, hence raises temperature, resulting in higher NOx. Conversely, low air fuel ratio inhibits complete combustion, resulting in high particulates. Good fuel economy favors complete and fast combustion, and tends to result in lower particulates. This is in correspondeance with the location of the points in Fig. 8 for the controllers run with low fuel consumption set points. The NOx-PM tradeoff limitation cannot be overcome by feedback control. The set points can control the location of the emissions on the NOx-PM curve, but cannot move the curve up or down. The points in Figure 8 are clustered by the type of set points used, rather than by controller, sensor set or controlled variable. This indicates that the set points are a major factor for emission results.

Since the fuel consumption values of all controllers were quite close, between 4.2 and 4.45 l/100 km, they will not be tabulated. Noteworthy is perhaps that the engine running open-loop has the worst fuel consumption of 4.55 l/100 km.

Transient data

This subsection shows some transient data for each of the controllers. Since part of the EUDC prescribes engine speeds outside of the range where mapping data was available, we concentrate on a 100 second time interval corresponding to the last big acceleration. This interval suffices to point out the interesting traits of all controllers.

Fig. 9 shows MAP and MAF for the PI controller on MAP and measured MAF. This controller outputs duty cycle commands for EGR and VGT actuators, hence position signals are omitted. The EGR and VGT control signals have very low frequency content, translating in a slow following of the transients. Due to the integral action, the steady state errors are zero. This is also true for the steady state errors outside of the mapped engine range. MAF overshoots in accelerations, which is conducive to fast torque response. It also implies low EGR rates, which correlates with the high NOx for this controller. MAP response is slow in transients. Since fast MAP response requires closing the VGT quickly, which impedes engine breathing and hence fast MAF response, there is a tradeoff in transient MAF and MAP response. This is also clearly visible in the subsequent controller plots.

Fig. 10 shows MAP and MAF for the PI controller on MAP and estimated MAF. As noted, the MAF estimator underestimates MAF in transients and overestimates MAF in high load conditions. The qualitative response of MAF is very similar to the PI controller on MAP and *measured* MAF. Here, MAF is higher due

to estimation errors, which correlates with higher NOx. Around $t = 1120$ sec the estimated MAF does not have time to converge to the set point due to integrator windup.

Fig. 11 shows MAP and MAF for the rank one controller.

This controller outputs desired EGR and VGT position, as opposed to duty cycle, and relies on a low level PI controller to regulate to the commanded positions. Since this controller was designed for maximum F_1 set points, these were the set points used. Steady state tracking is quite good, even though there is only one integrator. It was verified that MAP tracking is lost for minimum fuel consumption set points, fow which the controller was not designed. The high EGR levels bring exhaust and intake manifold pressures close together, which moves the flow characteristic of the EGR valve in a high gradient region: a small pressure disturbance has a large effect on flow. This shows up in the severe EGR valve oscillations atound $t = 1120$ seconds, which translate to the MAP and MAF signals through the coupling of the plant.

Fig. 12 shows EXMP and MAF for the CLF controller. The *measured* MAF signal and *not* the estimated MAF from the estimator was input into the controller, The controller is not supposed to track MAP (the corresponding gains were set to 0). This controller was designed for accurate transient MAF response, which is indeed quite visible in the figure. The EXMP response is accordingly slower. Due to the lack of integral action, the MAF error is nonzero for the first 10 sec, and the EXMP trace exhibits nonzero steady state error between $t = 1080$ and $t = 1100$. The fast MAF response is reflected both in the EGR and VGT control signal, due to the coupling of the controller. For the CLF controller the complete set point generation and gain calibration have been performed on the diesel engine model, after the gains had been set to constants. It is interesting to point out that about half of the 1.8 second interval with visible smoke occured on the tip-out at $t = 1075s$. Apparently, the MAF response is fast enough that the amount of air dropped before the actual injected fuel had decreased. Because the response is overdamped (no overshoot) and there is little effect of measurement noise, it seems that higher gains could have been used.

Fig. 13 shows MAP and EGR fraction for the PI controller on MAP and EGR fraction. Steady state tracking of MAP is quite good, but the integrator on EGR fraction is winding up at $t = 1050$ and 1115 seconds, which makes the transients very slow. This results in the EGR valve staying closed longer than it should, and the conmensurately high NOx in Table 2. Clearly, the antiwindup parameters need redesign for this controller.

Summary and Conclusions

The development and experimental validation of model-based control algorithms were described for a high-speed DI diesel engine with EGR and VGT. The controllers were developed and tested on the simulation model of the engine. Some additional fine-tuning of control parameters was done on the engine. The dSPACE rapid prototyping equipment allowed the same code to be used in simulation and experiment, resulting in a short turn around time.

We showed that the set point strategy is crucial to the closed loop performance. Indeed, the set points chosen largely governed the trade-off between NOx and particulate emissions over the European drive cycle for the controllers we tested. In the paradigm of set point regulating controllers, the feedback controller cannot do better then achieve the set point as best as possible. It is important to remember that the role of feedback control is to provide robustness and rapid transient response. The European drive cycle does not evaluate aggressive driving patterns, hence transient operation is not heavily emphasized in our comparison. It may also be that a set point strategy mandates a certain controller architecture, as in the case with the rank one controller.

Other important criteria by which to evaluate automotive controllers are the required sensor and actuator set, their computational load, and the calibration effort. Indeed, much of the calibration effort is spent in understanding the operation of the strategy. The requirement of a low computational load favors simple PI controllers on measured variables, where as little as possible of the engine model is implemented in the controller code. Engine models can enable a significant calibration effort reduction without increasing chronometric load. However, since control oriented engine models are still limited in accuracy, it is important to maintain a controller architecture that can be adjusted on the engine for final fine-tuning. We demonstrated the possibility of replacing the mass air flow sensor with an exhaust manifold pressure sensor, thereby achieving potential cost savings.

Acknowledgments

Mark Criddle, Paul Wood, and Mick Campbell of Visteon in Dunton operated the dyno used to obtain the data in this article. Charles Hawkins of Ford of Britain wrote the driver for the twin CAN cards. Jeff Cook from the Powertrain Control Systems Department at Ford Research Labs and Dave Pickman from Visteon, Dunton, initiated the project. We thank Darren Walker, Mary Breida, and Barry Powell for many useful ideas and discussions. We thank Jim Freudenberg and Rick Middleton for the useful discussions on feedback controller design.

Affiliations

- M.J. van Nieuwstadt: Ford Research Laboratory, Dearborn, Michigan.
- I.V. Kolmanovsky: Ford Research Laboratory, Dearborn, Michigan.
- P.E. Moraal: Ford Research Laboratory, Aachen, Germany.
- A.G. Stefanopoulou: Department of Mechanical and Environmental Engineering, University of California, Santa Barbara, CA 93106 Support is provided by the National Science Foundation under contract NSF ECS-97-33293; matching funds were provided by Ford Motor Company.
- M. Janković: Ford Research Laboratory, Dearborn, Michigan.

References

[1] , L. Guzzella, A. Amstutz, "Control of diesel engines," *IEEE Control Systems Magazine*, vol. 18, no. 5, pp. 53-71, 1998.

[2] , J.-P. Jensen, A.F. Kristensen, S.C. Sorenson, N. Houbak, E. Hendricks, "Mean Value Modeling of a Small Turbocharged Diesel Engine," SAE paper 910070, 1991.

[3] , M. Kao, J.J. Moskwa, "Turbocharged diesel engine modeling for nonlinear engine control and estimation," *ASME Journal of Dynamic Systems, Measurement and Control*, vol. 117, 1995.

[4] , N. Watson, "Dynamic turbocharged diesel engine simulator for electronic control system development," *Journal of Dynamic Systems, Measurement, and Control*, vol. 106, pp. 27-45, 1984.

[5] , I.V. Kolmanovsky, P.E. Moraal, M.J. van Nieuwstadt, A. Stefanopoulou, "Issues in modelling and control of variable geometry turbocharged diesel engines," *System Modelling and Optimization: Proceedings of the 18th IFIP Conference on System Modelling and Optimization*, Detroit, MI, Eds. M.P. Polis, A.L. Dontchev, P. Kall, I. Lasiecka and A.W. Olbrot, Chapman and Hall/CRC Research Notes in Mathematics, pp. 436-445, July 1999.

[6] , P.E. Moraal, M.J. van Nieuwstadt, I.V. Kolmanovsky, "Modelling and control of a variable geometry turbocharged Diesel engine," *COSY Workshop Proceedings of ECC 97, Brussels*, Brussels, 1997.

[7] , M. Janković, M. Janković, I. Kolmanovsky, "Robust nonlinear controller for turbocharged diesel engines," *IEEE Trans. on Control Systems Technology*, to appear.

[8] , A. Stefanopoulou and I. Kolmanovsky and J. Freudenberg, "Control of variable geometry turbocharged diesel engines for reduced emissions", *Proceedings of the ACC conference* Philadelphia, pp. 1383-1389, 1998.

[9] , M.J. van Nieuwstadt, P.E. Moraal, I.V. Kolmanovsky, A. Stefanopoulou, P. Wood, M. Criddle, "A comparison of SISO and MIMO designs for EGR-VGT control of a high speed diesel engine", *IFAC Workshop on Advances in Automotive Control*, Mohican State Park, Ohio, February 1998.

[10] , A. Stefanopoulou, I. Kolmanovsky, J. Freudenberg, "Control of variable geometry turbocharged diesel engines for reduced emissions," *IEEE Transactions on Control System Technology*, to appear.

[11] , "Bosch Automotive Handbook, 3rd Ed.," 1993.

[12] , R. Sepulchre, M. Janković, P.V. Kokotović, "Constructive nonlinear control", Springer-Verlag, London, 1997.

[13] , M. Janković, M. Janković ,I. Kolmanovsky, "Robust Nonlinear controller for turbocharged diesel engines," *Proceedings of the ACC conference*, Philadelphia, June 1998.

[14] , C. Arcoumanis, A. Megaritis, "Real time measurement of particulates in a turbocharged DI diesel engine," SAE paper 922390, 1992.

[15] , A.C. Alkidas, "Relationships between smoke measurements and particulate measurements," SAE paper 840412, 1984.

[16] , G. Greeves, C.H.T. Wang, "Origins of diesel particulate mass emission," SAE paper 810260, 1981.

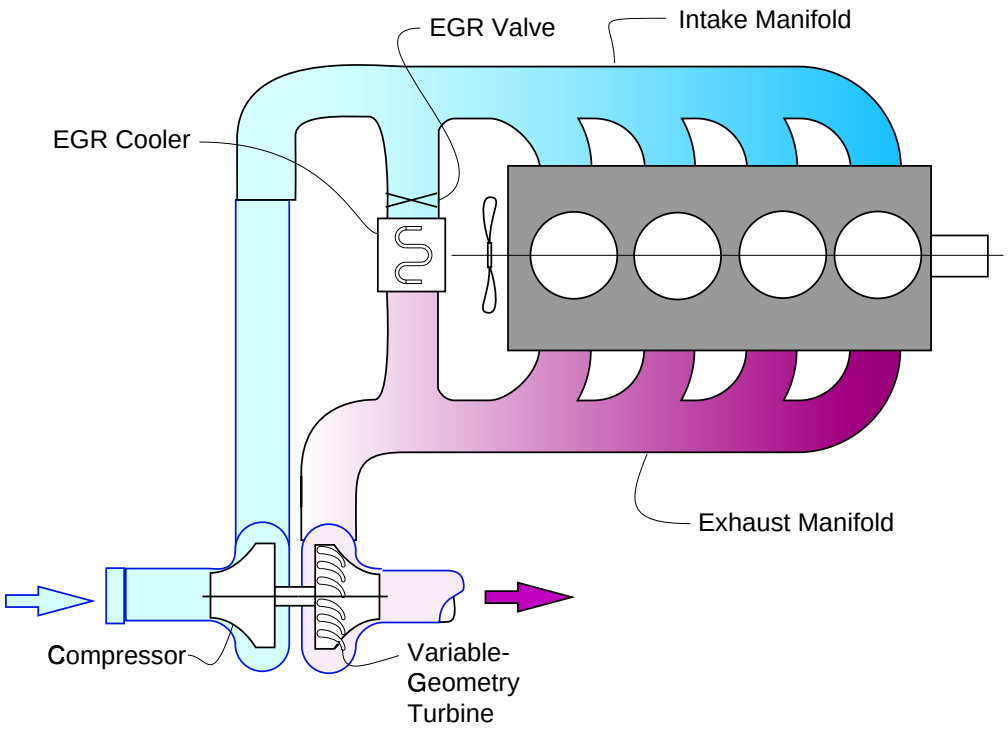

Figure 1: Diesel engine configuration.

1 FIGURES

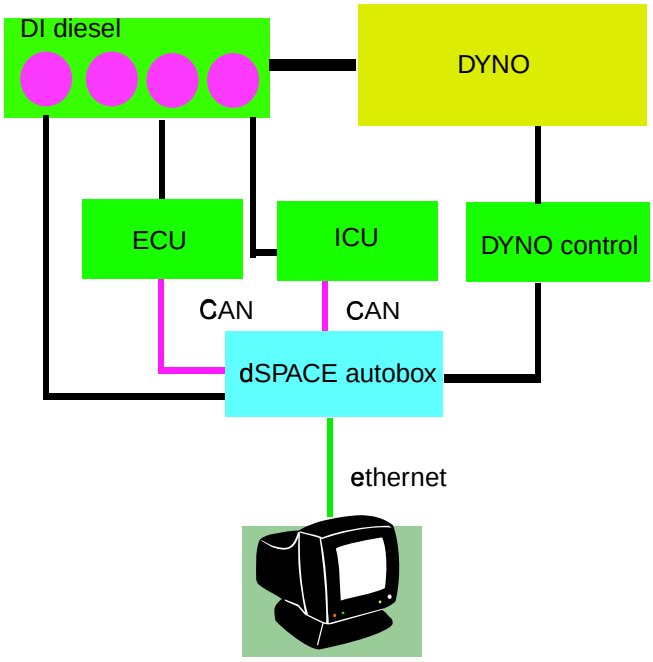

Figure 2: Harware setup.

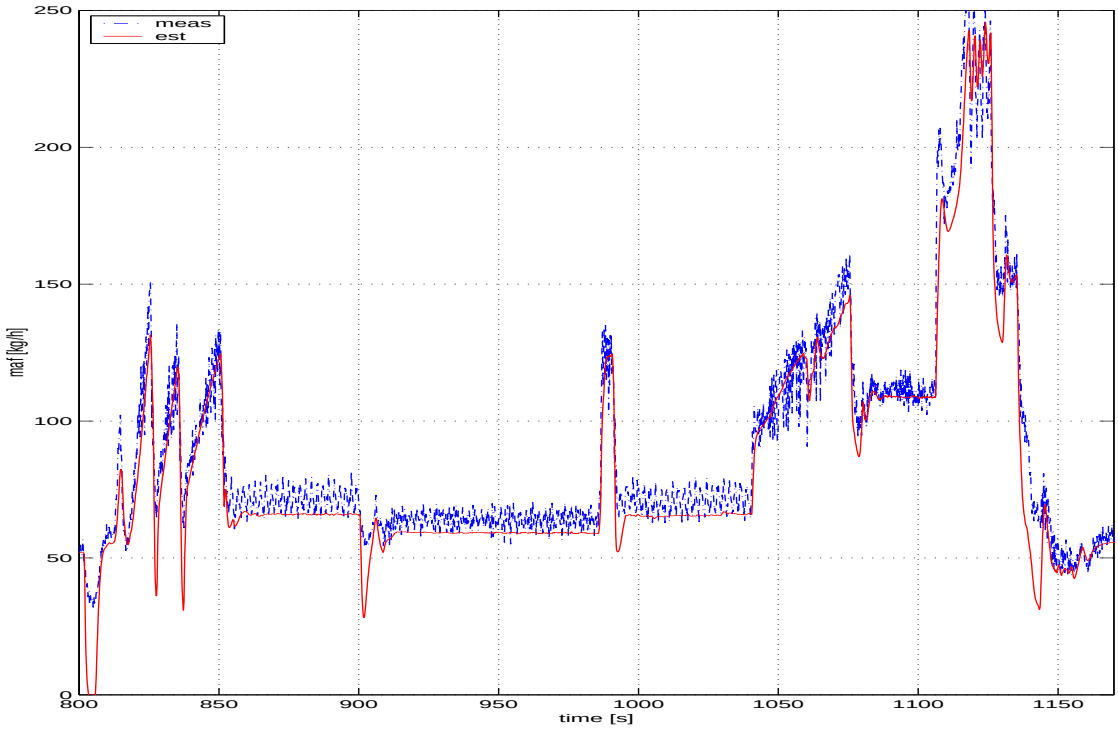

Figure 3: MAF estimator over the European drive cycle.

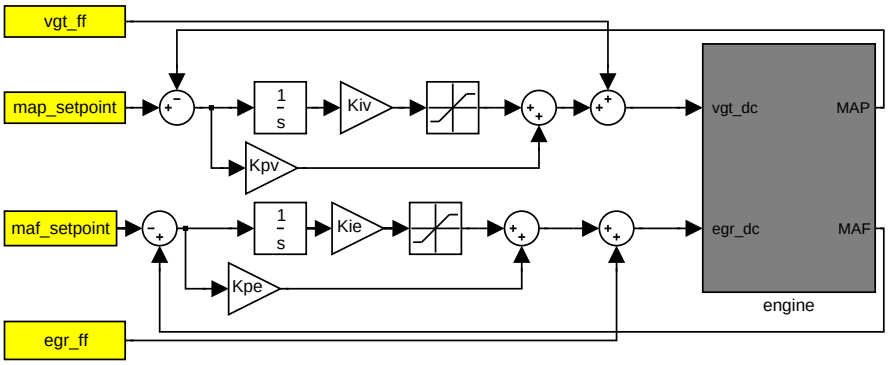

Figure 4: Architecture for PI controller on MAP and MAF.

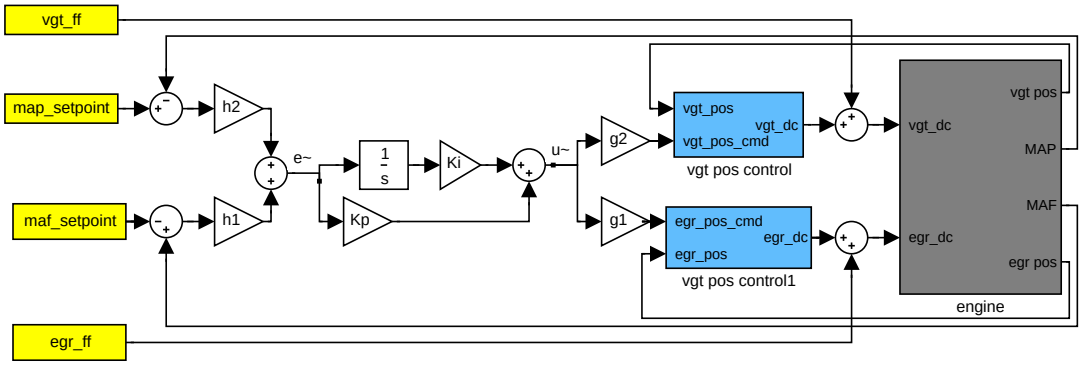

Figure 5: Rank one controller architecture.

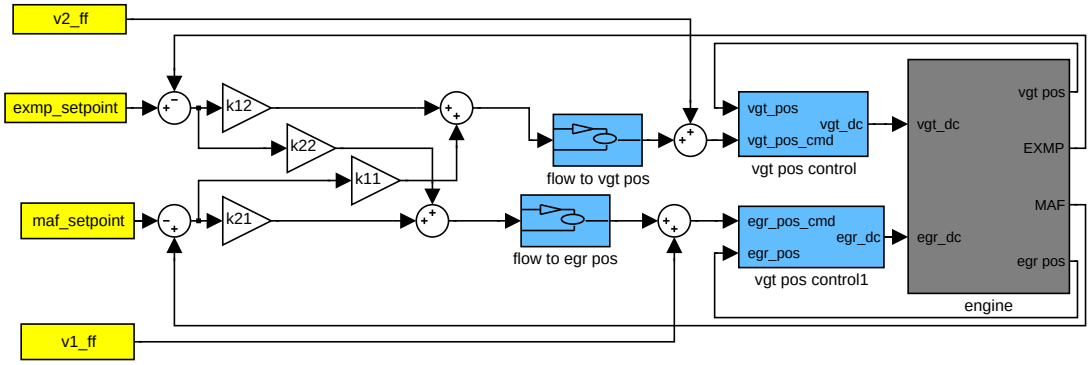

Figure 6: Block diagram of the CLF controller.

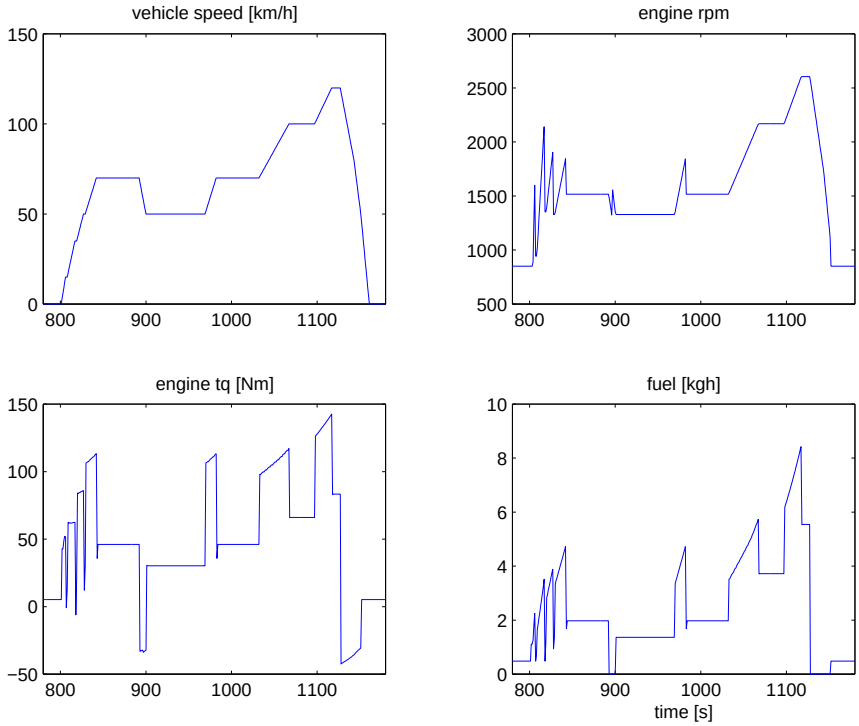

Figure 7: EUDC: vehicle speed, engine speed, engine load, requested fuel.

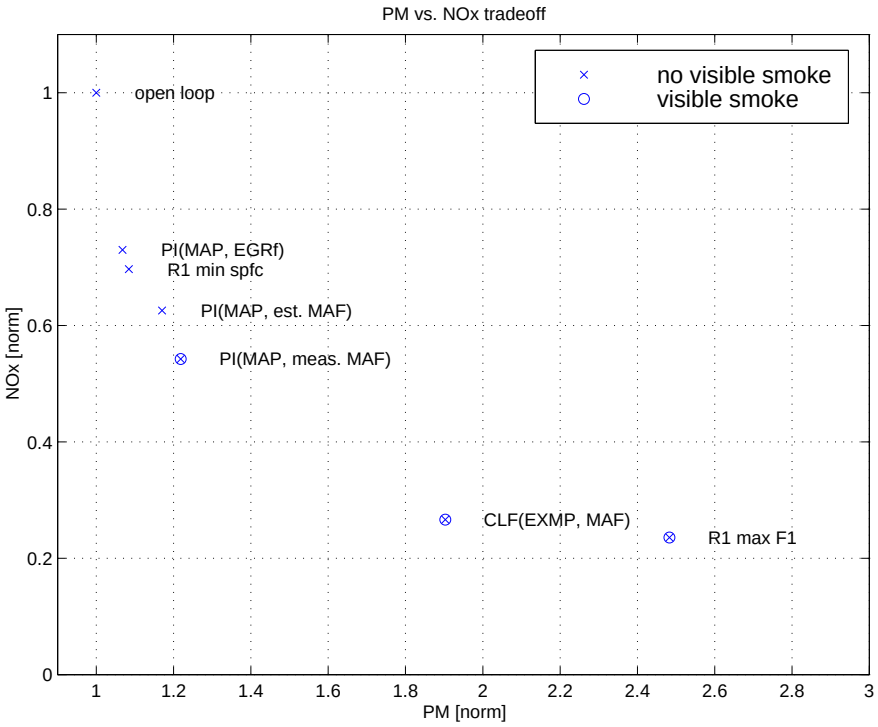

Figure 8: NOx-particulate matter tradeoff.

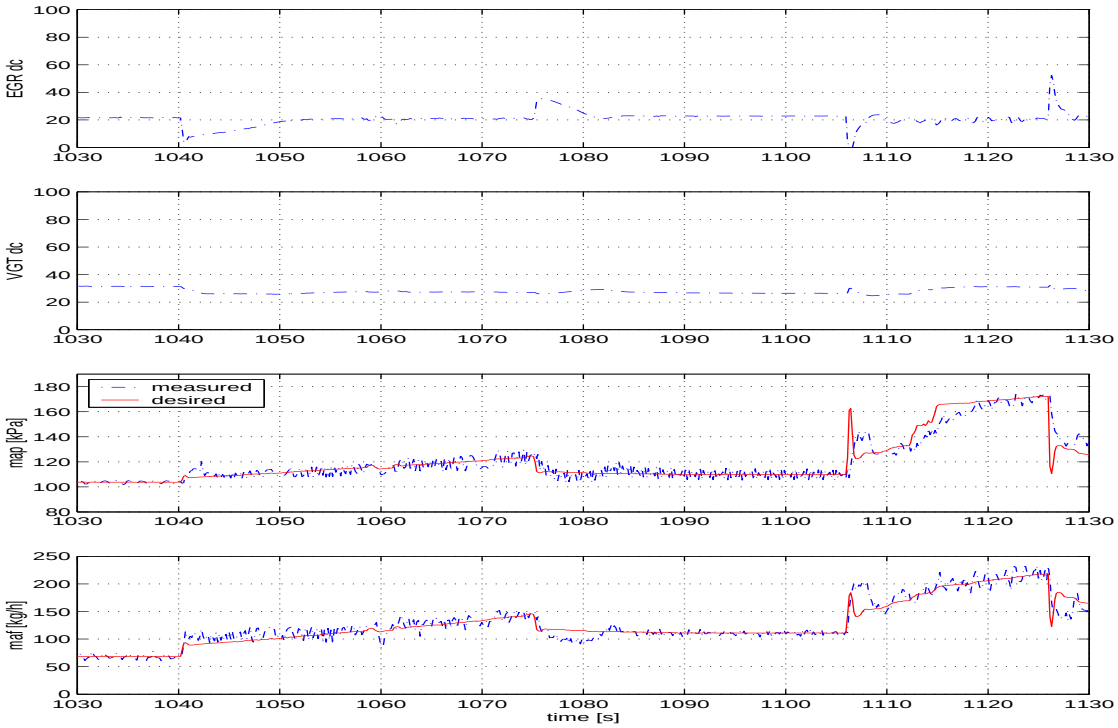

Figure 9: MAP and MAF for the MAP-measured MAF controller.

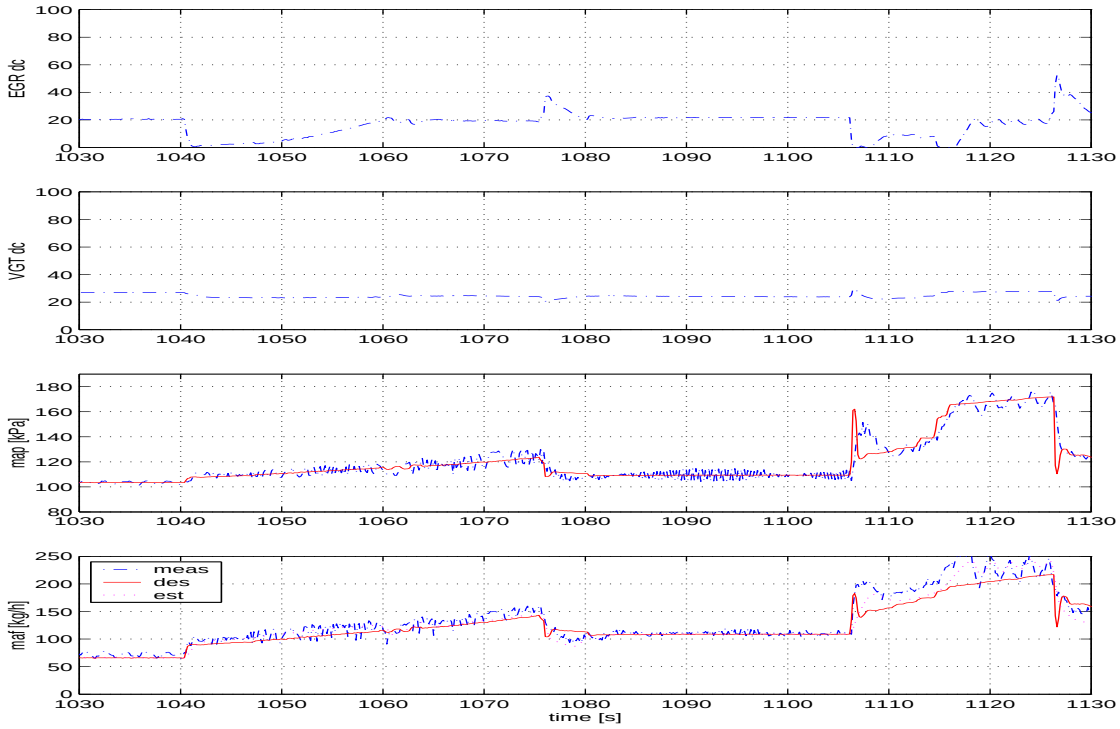

Figure 10: MAP and MAF and estimated MAF for MAP-estimated MAF controller.

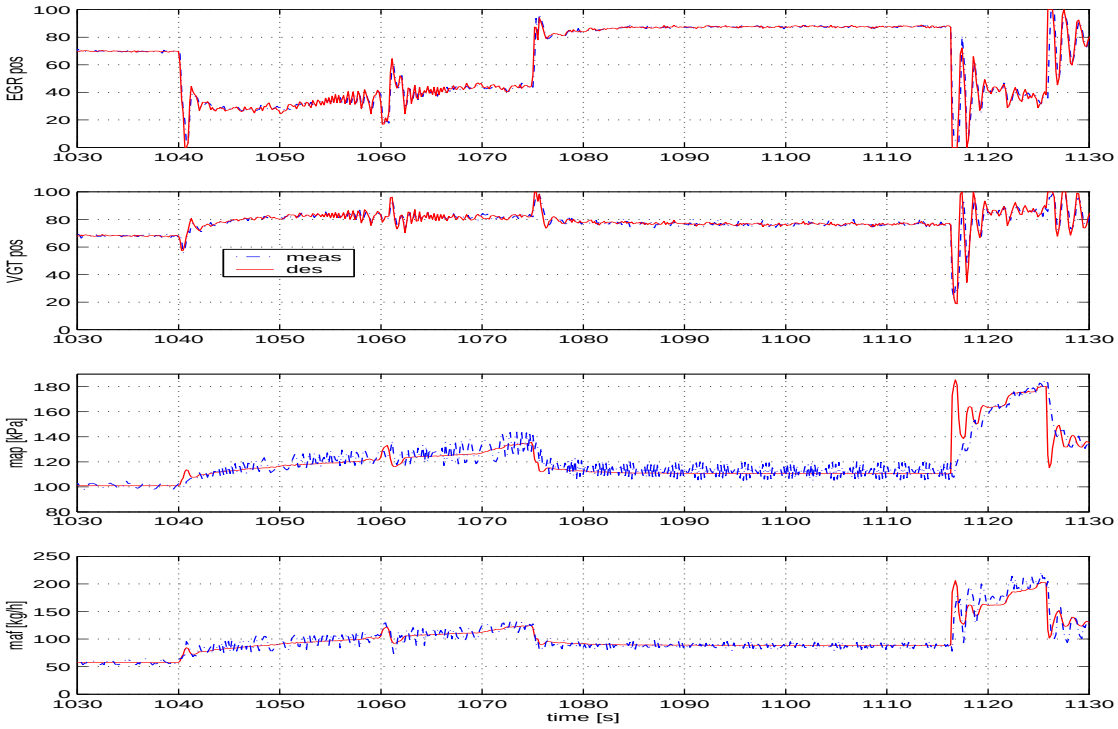

Figure 11: MAP and MAF for the rank one controller. Set points for maximum F1.

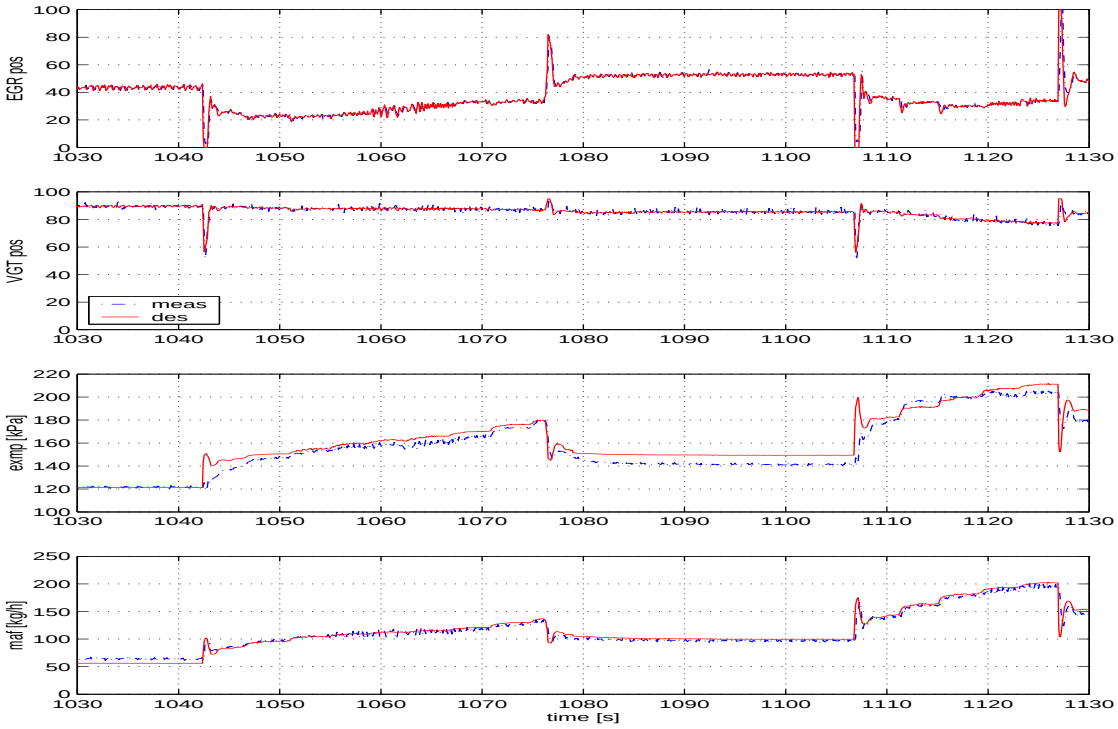

Figure 12: MAF and EXMP for the CLF controller.

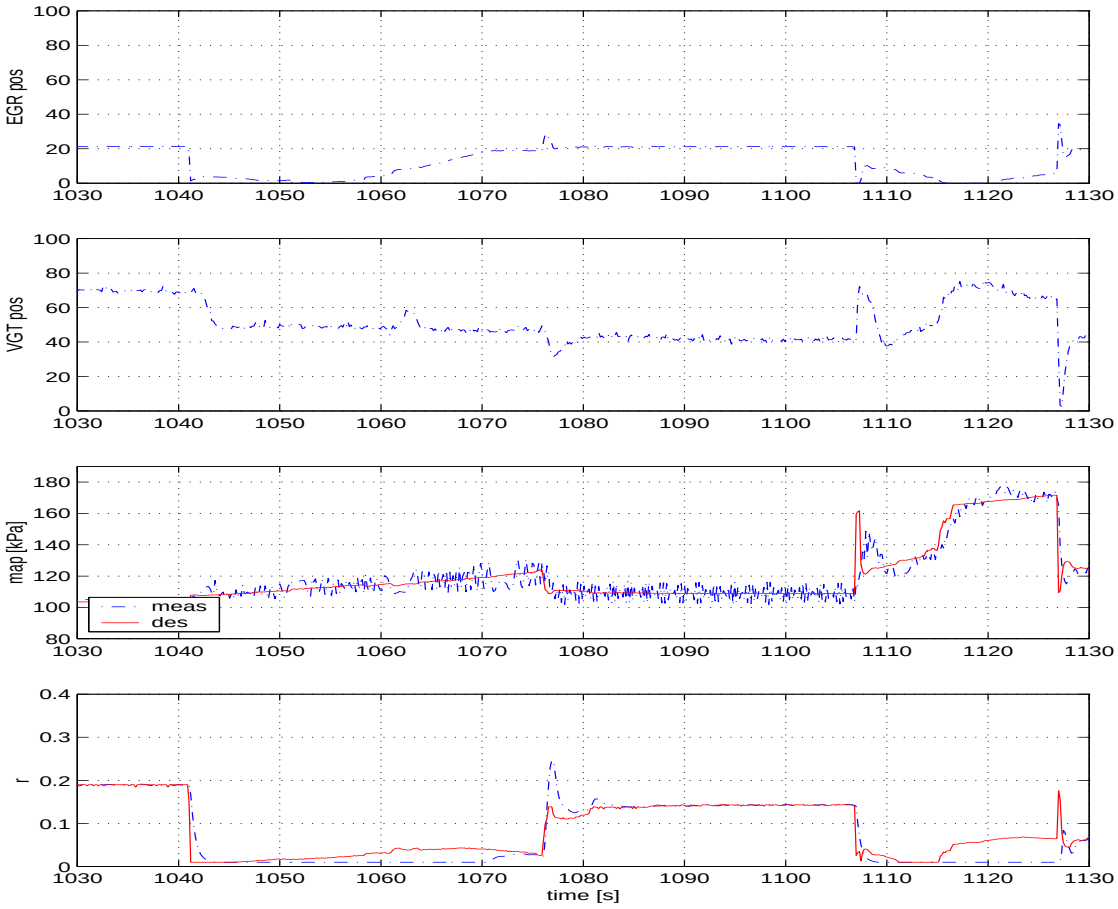

Figure 13: MAP and EGR fraction for the PI controller on MAP and EGR fraction.

Controller (controlled variables)	integrators	type	output	measured variables	coupled	computational load
PI(MAP, meas MAF)	2	PI	duty cycle	(MAP, MAF)	No	lower
PI(MAP, est MAF)	2	PI	duty cycle	(MAP, EXMP)	No	higher
R1(h_1MAF+h_2MAP)	1	PI	position	(MAP, MAF)	Yes	lower
CLF(MAF, EXMP)	0	P	flow	(MAF, EXMP)	Yes	higher
PI(MAP, EGRf)	2	PI	duty cycle	(MAP, EXMP)	No	higher

Table 1: Controller summary.

2 Tables

Controller:	section	tot NOx	tot THC	tot CO	smoke [sec]	tot PM
open loop		1.0000	1.0000	1.0000	0.0000	1.0000
PI(MAP, meas MAF)		0.5423	1.1052	1.0668	0.0500	1.2179
PI(MAP, est MAF)		0.6256	1.0551	0.9333	0.0000	1.1699
R1 minspfc		0.6969	1.0107	0.9458	0.0000	1.0842
R1 maxF1		0.2357	1.1723	1.6949	26.3000	2.4819
CLF(EXMP, MAF)		0.2664	0.9843	1.1105	1.8000	1.9019
PI(MAP, EGRf)		0.7299	1.0088	0.8391	0.0000	1.0671

Table 2: Emissions for various controllers over EUDC. Emissions are normalized with respect to open-loop.